ACI STRUCTURAL JOURNAL TECHNICAL PAPER

Title No. 121-S73

Dowel Bar Contribution to Bond Deterioration under Cyclic Loading

by Edom A. Zewdie, Chikako Fujiyama, and Koichi Maekawa

This research delves into the performance of dowels in reinforced concrete joints, highlighting the crucial role of subgrade reaction in providing firm support for dowel bars. The experimental analysis conducted on jointed specimens loaded below their dowel capacity revealed permanent deformations. The examination discerned a gradual extension of cracks emanating from the joint interface, attributing their initiation to bond deterioration under cyclic loading conditions. This research encompasses diverse variables, including dowel arrangements, bar sizes, types, confinement levels, bond conditions, and section size, offering a comprehensive exploration of factors influencing this different joint behavior.

Keywords: bond deterioration; crack; cyclic shear; dowel; joint interface; premature failure; splitting failure.

INTRODUCTION

In reinforced concrete structures, joints serve as a critical shear transfer zone. Joint interfaces alter between flat (smooth/very smooth), rough crack, or mechanically interlocking. These interfaces are due to the connection of precast concrete construction, jointed concrete pavements, retrofitted concrete columns, the interface between old and new concrete, flexural-shear cracks formed in ultimate limit states, and so on. Researchers[1-3] indicate that the shear transfer mechanism across joint interfaces is the contribution of mechanical interlocking, aggregate interlocking, axial confining stress, bar pullout displacement, bar pullout force, concrete resistance, and dowel action. These mechanisms coexist and have demonstrated interdependence. Their interaction depends on the number of reinforcements crossing the interface, bar size, reinforcement bar property, and strength of concrete. Overall contribution is difficult to obtain by simple superposition; hence, a wide range of shear models and scatter of experimental results exist.

The shear transfer mechanism according to Maekawa et al.,[2] is summarized in Fig. 1. Herein, displacement δ caused by the shear load is refrained by the normal stress and shear stresses along the two directions. Normal stresses are induced normal to the crack plane due to the resistance of the aggregate interlocking effect. This aggregate interlocking is responsible for the crack widening at the interface. Due to the crack widening, the bar is displaced, and tension is created on the bar. This pullout tension force is resisted by the compressive force. The crack opening not only depends on the degree of roughness, but also on the level of axial confinement and the controlling mechanism of this axial confinement. Parallel to the crack plane, shear stress resistance is due to dowel action and concrete resistance to shear. For flat (very smooth) interfaces, shear capacity is governed by dowel strength. In the absence of dowels, it is reported[1] that reinforced concrete (RC) joints behave in a brittle manner with joint slips less than 0.05 mm (0.00197 in.). It is considered that ductility is exhibited in the presence of dowels and failure occurs at larger slips of 0.5 to 1.5 mm (0.02 to 0.05 in.).[1]

The ultimate shear capacity of RC joints depends on the failure criterion imputed to section property and loading conditions. According to researchers,[2,4] there are three governing modes of failures for RC joint interfaces. Failure mode 1 is due to concrete spalling and plastic hinge formation; this is initiated due to the plastic hinge at a certain location away from the joint interface. Mode 2 is due to insufficient cover provision, leading to weak and strong mechanisms. In a weak mechanism, failure is due to the inability of the cover to resist the tensile stress developed when the bar pushes the concrete cover. The strong mechanism is where the bar is pushed against the concrete core, and no splitting is expected to occur. The final mode of failure is when the joint interface is flat. In this case, the shear capacity of the joint depends on the dowel strength of the bars. Herein, the pullout of reinforcing bars is negligible, and strength depends on the dowel strength of the bars.

The contribution of dowel action is overlooked due to the difficulty in exploring its contribution. This is caused because of the difficulty in quantitatively measuring shear force transferred by the integration of the different components. Embedded bars in concrete experiments are used to investigate critical dowel load and concrete subgrade stiffness. This concrete subgrade reaction is detrimental to the accurate relationship between the deflection, bar strain, and concrete local fracturing. The Timoshenko[5] beam on elastic foundation analogy is adopted; some suggested a uniform stress distribution under the bars, and others[4] took the bearing capacity of the subgrade stiffness to be several times higher than the uniaxial compressive strength of concrete. Thus, both critical dowel capacity and concrete subgrade stiffness are empirically formulated. Despite the differences in the subgrade stiffness of the supporting concrete, critical dowel load predictions[1,4,6] are similar.

The aforementioned cases already made the shear transfer mechanism complex. Most experiments consider

ACI Structural Journal, V. 121, No. 5, September 2024.

MS No. S-2023-180.R3, doi: 10.14359/51740858, received February 6, 2024, and reviewed under Institute publication policies.

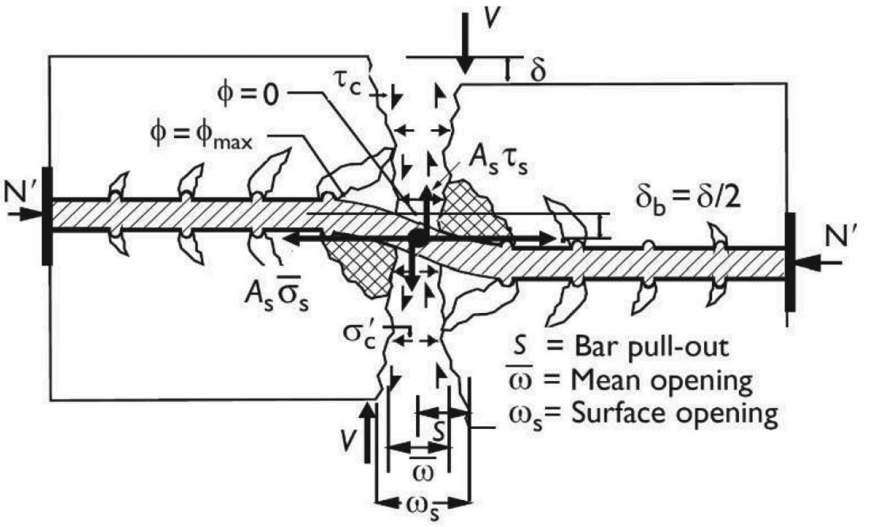

Fig. 1—Summary of shear-transfer mechanism.[2]

monotonically loaded specimens. Cyclic loading is considered in some cases, but is limited to addressing dowel stiffness degradation after plastic hinge formation. In this research, a loading condition less than the critical and design dowel capacity is cyclically applied. Concrete deterioration is observed under this cyclic loading. This cyclic degradation strongly affected bond loss and finally led to splitting cracks, joint deteriorations, and plastic hinge formation.

RESEARCH SIGNIFICANCE

Experimental investigations and the performance of existing structures exhibit considerable variation. For instance, in jointed concrete pavements, bridge corbels, deep beams, and piles, cases of early concrete deterioration under service conditions are observed. Structural members with no axial confining pressure are experimentally simulated in this research. An experimental investigation to address the effect of cyclic loading degradation on the section's capacity is considered. Stepwise, incremental cyclic loads beginning from less-than-critical dowel load are applied to the specimens. Under these conditions, failure criteria for the specimens are studied and presented in this paper. Herein, the initiation of failure due to the debonding of bar and concrete is duly given attention. This information is important for the prediction of RC structures' performance under cyclic loading.

The durability of joints in RC structures is notably influenced by cyclic shear loading. Precise predictions of the shear transfer behavior enable accurate estimation of structures' remaining life, enhancing structural performance and facilitating the development of ultra-high-performance construction materials. Consequently, it contributes to enhancing the performance of joints, increasing safety against collapse, and creates opportunities for the implementation of engineered materials.

TEST PROGRAM

Despite rigorous experimental investigations, the intensity and behavior of loading experienced on existing structures is different from the laboratory mockups. Experiments of different arrangements can facilitate the investigation of different governing criteria. The experimental layout for an embedded bar under shear loading depends on the objective and factors affecting it. In general, it can be categorized into loads directly applied to the dowel and loads applied to the concrete unit. In this investigation, jointed specimens with two very smooth joints are constructed. A load is applied to the center unit of these jointed specimens (Fig. 2). The applied load is resisted by two steel plate supports near the very smooth interface. Hence, the load is transferred to the supports by the two dowel actions on the left and right.

Rectangular RC beams are prepared with two flat (very smooth) joint interfaces. Test specimens (Fig. 2) consisted of three concrete units crossed with reinforcing bars. At the joint interfaces, polytetrafluoroethylene sheets are placed to avoid any frictional stress transfer between the units. The length of embedment of the dowel bars extends all the way through the three concrete units. The embedment lengths used are 600 and 300 mm (24 and 11.81 in.). Specimens of different bar types, bar sizes, cross section sizes, confinement types, and bond conditions are organized as shown in Fig. 2. In Fig. 2, Beams 1, 1R, and 2 are specimens made with a single embedded bar. Beams 1 and 1R are RC sections embedded with deformed bars (bars with lugs), while Beam 2 is an RC section made with a plain bar. Beams 3 and 4 are RC sections with different bar sizes and concrete cross section sizes, respectively. Beams 4 and 8 are twice the size of Beam 1, and the length of the loading plate (L) is altered (Fig. 1) from 150 to 250 mm (6 to 9.9 in.). In addition, the embedded length of the bar for Beam 8 is 300 mm (11.81 in.). Confined specimens (Beams 5 and 6) are constructed by using spiral stirrups. For Beams 5 and 6, two different stirrup arrangements are used. In Beam 5, active confinement with direct contact of longitudinal and stirrups is adopted, whereas Beam 6 has passive confinement with no direct contact in the longitudinal and stirrups. In Beam 7, the reinforced bar is lapped with rubber of 1 mm (0.0394 in.) thick into 10 layers. This removes the bond in the rubber-covered region and creates a weak subgrade stiffness. In all the specimens, the center unit is 300 mm

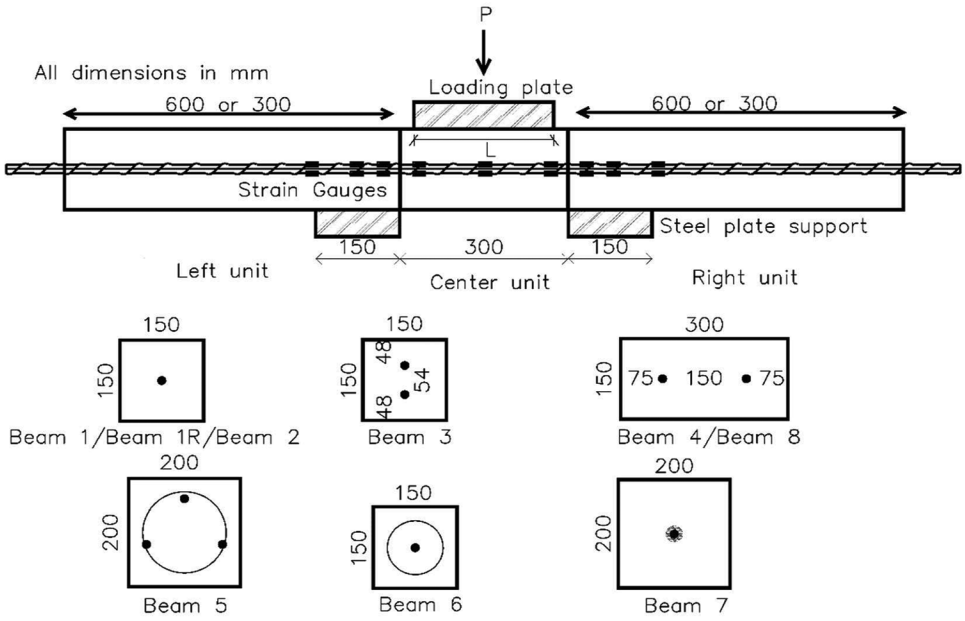

Fig. 2—Specimen layout and dimensions.

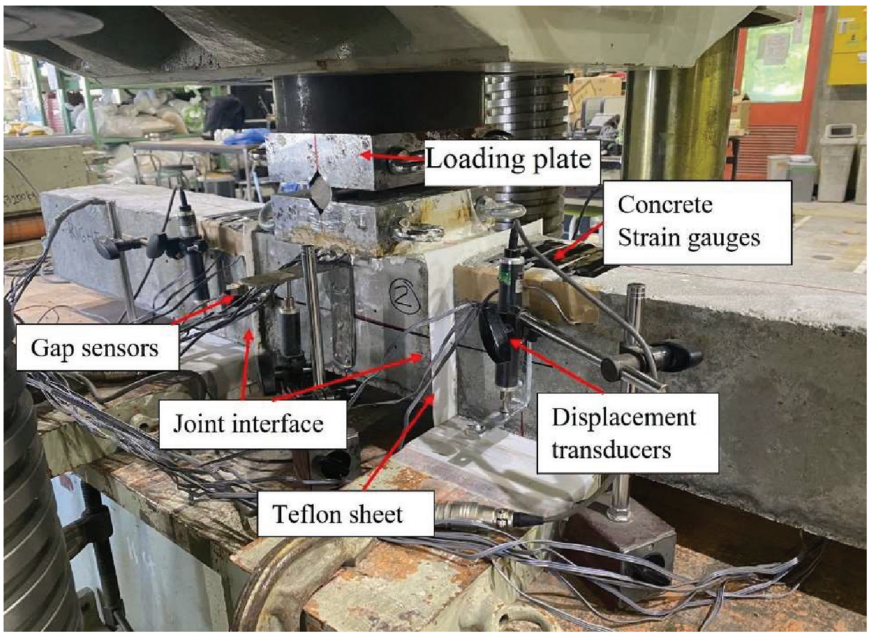

Fig. 3—Experiment setup and measuring instruments.

(11.81 in.) in longitudinal length. The left and right units are each 600 mm (24 in.) long for all the specimens except Beam 8. Details of the specimens' dimensions, loading plate, and bar arrangement are presented in Fig. 2.

To measure strain variation on the reinforcing bar and local strain variation between different locations on the reinforcement bar, strain gauges are mounted (Fig. 2). These strain gauges are placed *D* distances from the joint interfaces. The Beam 8 reinforcing bar is installed with no strain gauges. With the exception of Beams 1 and 2, in all the other specimens, concrete strain gauges are placed at the surface of both the left and right units near the joints. In addition, displacement transducers and gap sensors are used to measure relative vertical displacements (δ) and joint openings, respectively (Fig. 3). The displacement transducers are placed at the center and support to measure the joint displacement of the vertical slip due to the cyclic shear. The gap sensors installed at the joint interfaces are placed to measure opening due to the cyclic shear load.

Materials

Very smooth concrete joints at the interface are achieved by casting the center units first and then performing a subsequent casting of left and right units after sufficient curing. Concrete cylindrical specimens are sampled for each mixture, and compressive strength is described in Table 1. All concrete blocks are made of ordinary portland cement with a maximum size crushed aggregate of 20 mm (0.79 in.). The specimens are cast and air-cured in the laboratory, covered with plastic. For Beam 8, only mortar grout is used to cast

Table 1—Concrete properties

Specimen	Longitudinal bar size, mm	Stirrup bar size, mm	f_{yk}, MPa	Left unit	Center unit	Right unit
				Compressive strength, MPa		
Beam 1	16	—	400	29	37	29
Beam 1R	16	—	400	65	54	65
Beam 2	16	—	400	39	36	39
Beam 3	13	—	385	37	57	37
Beam 4	16	—	400	45	57	43
Beam 5	13	8	385	49	57	43
Beam 6	16	8	400	48	57	48
Beam 7	16	—	400	42	57	42
Beam 8	16	—	400	64	78	64

Table 2—Dowel capacity of specimens

Specimen	f_{yk}, MPa	D_u, kN	$D_{u,d}$, kN	Description
Beam 1	400	36	27	Control specimen
Beam 1R	400	49	37	Lower load level, higher compressive strength
Beam 2	400	40	30	Round bar
Beam 3	385	57	43	Two bars with a smaller diameter
Beam 4	400	87	67	Double cross section size
Beam 5	385	85	65	Active confinement
Beam 6	400	46	35	Passive confinement
Beam 7	400	—	—	No bond, rubber lapped, and monotonic loading
Beam 8	400	106	82	Double cross section size, mortar mixture, highest compressive strength, short embedment length, and no strain gauges

the specimens. The concrete compression tests on 200 mm (7.9 in.) height x 100 mm (3.9 in.) diameter cylindrical specimens were carried out before or after all test series. The mortar compression test samples are taken by using 100 mm (3.9 in.) height x 50 mm (2 in.) diameter cylindrical specimens. Sixteen and 13 mm (0.62 and 0.51 in.) longitudinal bars of 400 and 385 MPa (58 and 56 ksi) strength are used, respectively (Table 1).

Loading

To set the loading criteria, the critical dowel capacity and design capacity of the section were computed. Dowel capacity equations, according to Vintzēleou and Tassios[4] and Randl,[1] are used to calculate the capacity of the section. The dowel capacity for each section is computed based on Eq. (1) and (2). The critical dowel load (Eq. (1)) and design dowel capacity (Eq. (2)) of the beams are presented in Table 2. For computation of the critical dowel load, the lowest compressive strength from the three units is selected. All specimens except Beam 7 are subjected to cyclic loading. The cyclic loading applied to the joints is less than the dowel capacity of the sections presented in Table 2. The loading history adopted for each of the specimens is presented in Fig. 4. The load amplitude and the number of cycles applied to each of the sections vary. This is due to manual control of the speed dial and load indicator gauge to maintain controlled loading conditions. While maintaining precise control over the load amplitude during the successive loading proves challenging, cyclic loading is applied, accompanied by a gradual increase in load amplitude after a series of cycles

$$D_u = 1.3D^2\sqrt{f_{ck}f_{yk}} \quad (1)$$

$$D_{u,d} = D^2\sqrt{f_{ck}f_{yk}} \quad (2)$$

where D_u is critical dowel capacity; D_{ud} is design dowel capacity; D is reinforcing bar diameter; f_{ck} is the characteristic compressive strength of concrete; and f_{yk} is the characteristic yield strength of the reinforcing bar.

EXPERIMENTAL RESULTS AND DISCUSSION

Bond deterioration

The cyclic load applied at the center unit of the specimens results in progressive damage of the jointed specimen. This progressive damage starts at the joint interface and gradually progresses to the surface of the specimen. Figure 4 shows the load-displacement relationship of the specimens herein; it is observed that the beams undergo cyclic concrete degradation. A residual displacement is present after each cycle of loading. The sum of the residual deformation added after each cycle gives the cumulative damage of the section (Fig. 5). In the computation of this residual deformation (cumulative damage), the initial damage in the section due to the initial loading is not considered. In this initial loading stage, some bedding error is observed, which could be due

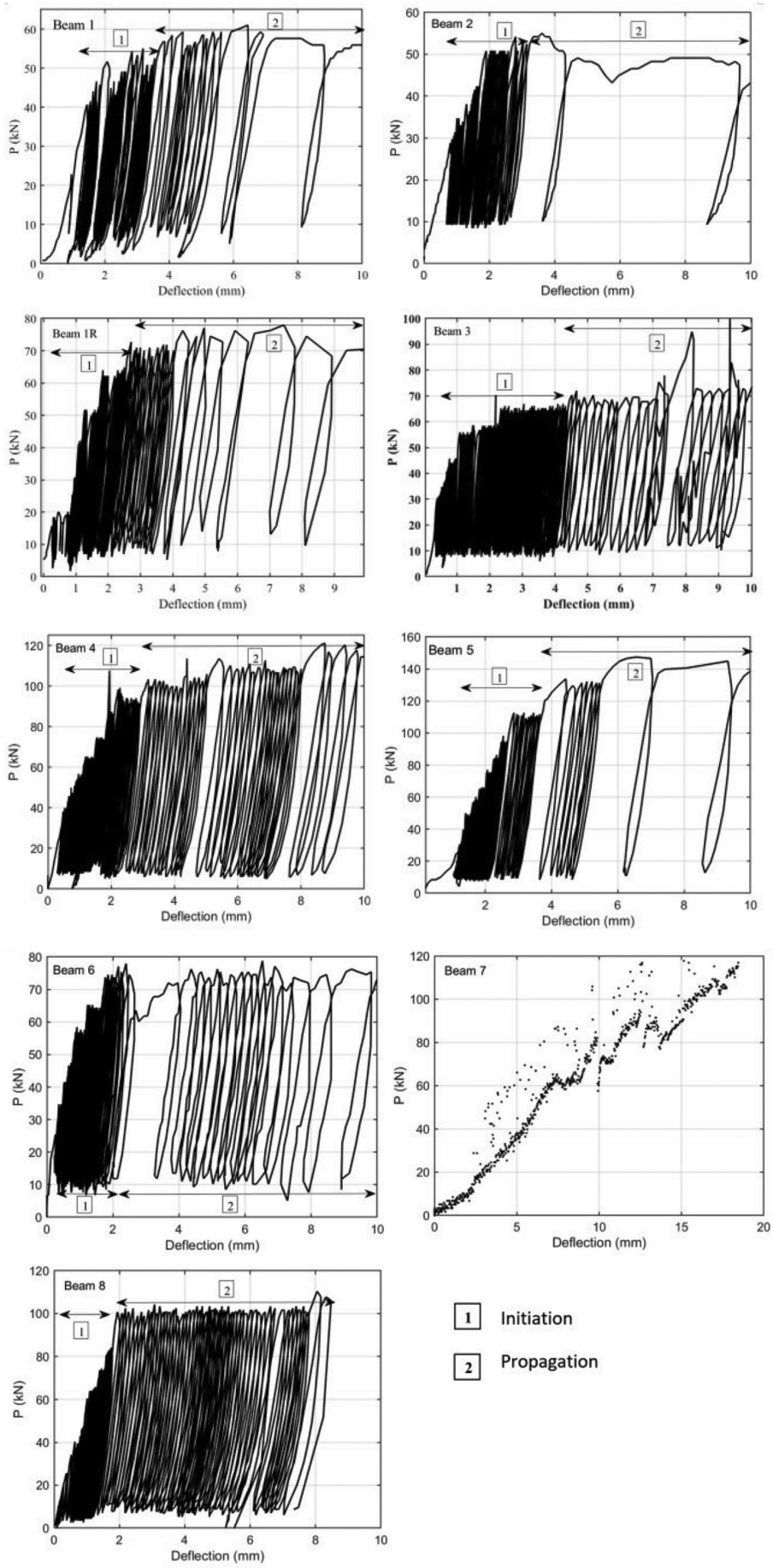

Fig. 4—Experiment results of specimens.

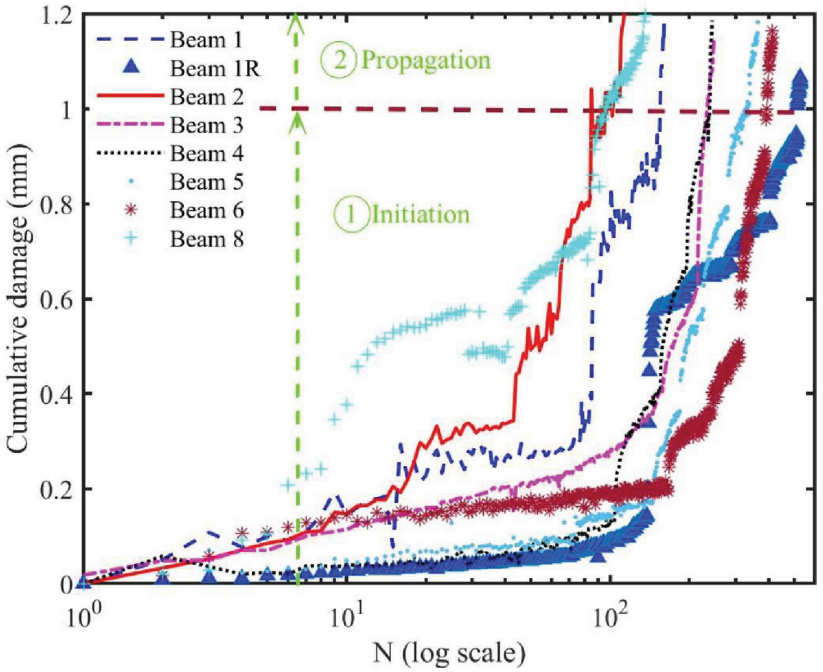

Fig. 5—Rate of damage of specimens.

to the strain gauge protective layers. These layers are applied to protect the strain gauge from moisture and damage while casting the concrete. The bedding error observed reduces when the layers are reduced and tightly placed. The section with no strain gauge (Beam 8) also confirms that such errors do not appear without the layers. The cumulative damage versus the number of repetitive cycle loading (N) for each specimen is plotted in Fig. 5. The damage rate of the specimens is found to have exponential growth (Fig. 5). The rate of damage presented in Fig. 5 shows that damage is highly incremental even if the load is less than the expected dowel capacity. The plasticity of the sections observed in Fig. 4 is attributed to concrete degradation. This has led to premature failure due to concrete degradation in the experimental specimens (Fig. 6).

The patterns of the load-deflection diagram can be grouped in two. The first category, where the rate of damage is low and there is congestion in the load deflection diagram, is categorized as the crack initiation stage. The second category, where there is significant plasticization, is categorized as the crack propagation stage. Concrete degradation on the crack propagation stage depends upon the different tested parameters. The crack propagation stage is different under the different tested conditions. As the load-deflection curve for the specimens in Fig. 4 showed a variation in the propagation stage, the observed crack propagation and fracture behavior for the specimens are also different. The crack initiation stage is the initial cause of the progression of a crack in the later stage. During the initiation stage, bond deterioration occurs, playing a crucial role in the subsequent progression of cracks in later stages.

Unconfined sections with deformed bars (Beams 1, 1R, 3, and 4) displayed splitting cracks at the top and bottom face of the specimen. This splitting failure originated from the bar at the position of the joint interface (Fig. 6). The surface splitting observed on Beams 1 and 3 progresses throughout the length of the specimen. This crack propagates along the bar axis. On the contrary, the splitting crack observed on Beam 4 does not follow the bar axis, but moves toward the edge of the specimen (Fig. 6). Damage of the section with plain bars (Beam 2) shows that the section collapses with side cracks and no splitting failures (Fig. 6). Figure 4 shows that the section displays progressive damage of concrete under cyclic loading below its capacity. The contribution of bar lugs under the cyclic load application can be understood by comparing Beams 1 and 2. For the crack propagation stage, the specimen with a plain bar shows significant deflection, leading to collapse. The strain values at 2D for the plain bars are higher as compared to Beam 1 (Fig. 7). Thus, Beam 1's fatigue capacity is increased due to the presence of bar lugs (Fig. 8).

Confined sections (Beams 5 and 6) displayed concrete deterioration near the joint interface (Fig. 5). In Fig. 4 and 5, confinement is shown to lengthen the crack initiation stage. Thus, increased fatigue performance is obtained. The propagation stage for Beams 5 and 6 is different due to the different confinement techniques applied. In both the specimens, the concrete deterioration is close to the joint interface. The strain gauge reading for these specimens confirms the existence of bond loss. The cyclic loading also resulted in cyclic strain increments, which is responsible for the bond loss. The bond loss near the joint face is responsible for the plastic hinge formation of the bars. This stage is accompanied with significant crack propagation near the joint interfaces.

Beam 8 displays early concrete deterioration near the joint interface (Fig. 6). No strain gauge is placed in this specimen, thus confirming the bond deterioration is not caused due to the strain gauge adhesives. Figure 4 shows cyclic loading also resulted in cyclic damage, which is responsible for the bond loss. This stage is accompanied by significant crack

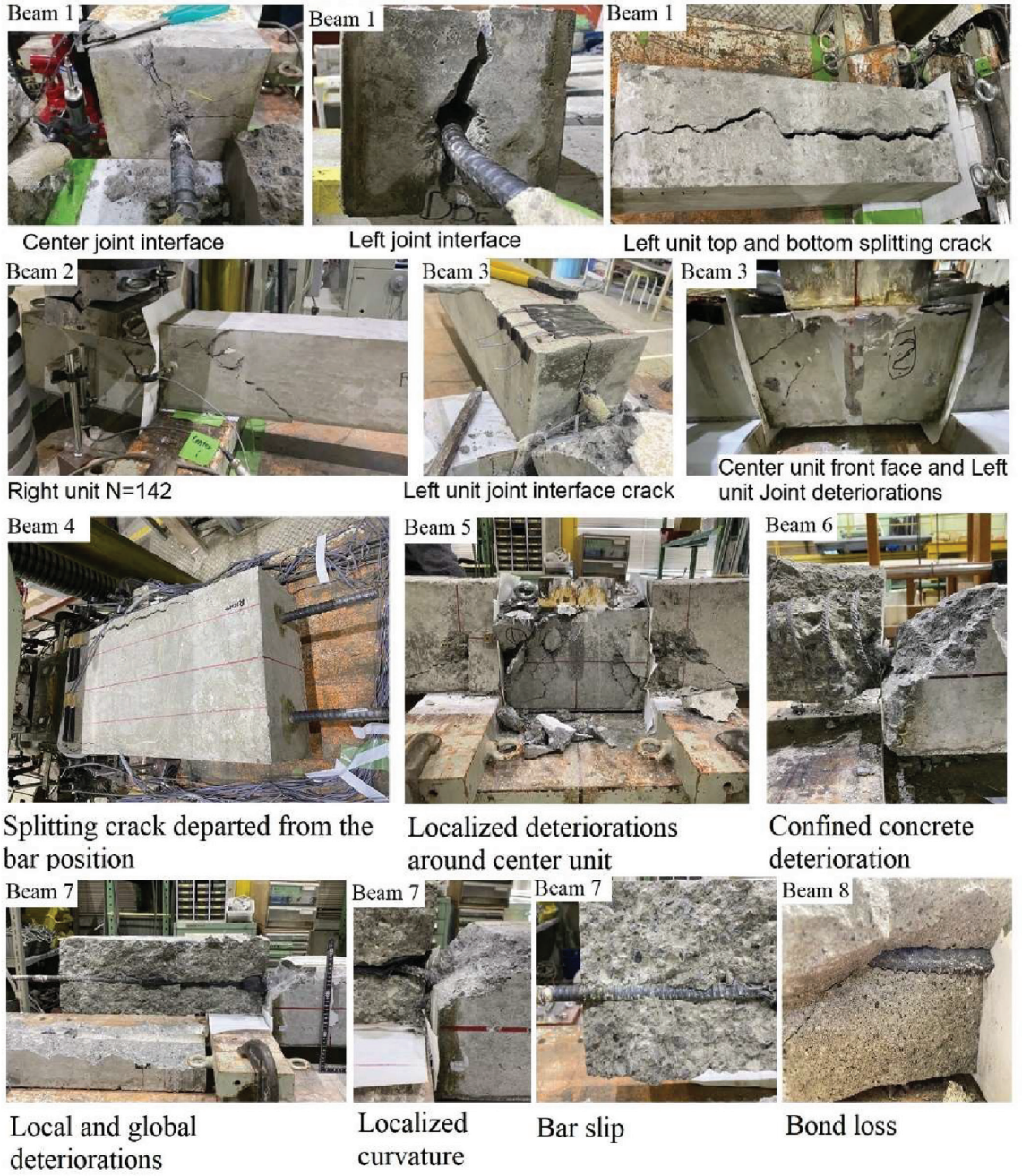

Fig. 6—Premature section failures observed on specimens.

propagation near the joint interfaces. Even if the capacity of the section increased by doubling the section (Beam 1) and the compressive strength of the specimen increased by using mortar grout only, the section deteriorates fast (Fig. 8).

The load-deflection curves for all the specimens show almost parallel loading and unloading curves. This implies that the stiffness of the section is not affected by the cyclic loading. As shown in Fig. 4 with the stiffness not being affected, the cyclic deterioration progressed. According to Timoshenko's[5] beam on elastic foundation theory, the continuous reaction of the foundation is proportional to the deflection. This constant is defined as subgrade stiffness and is the reaction per unit length when deflection is equal to unity. In this experiment, constant k values are obtained. But a permanent deformation exists; thus, the experimental RC sections fail to agree with the beam on elastic foundation theory. This can be attributed to the subgrade's brittle behavior.

The joint deteriorations observed in the specimens initiate due to local bond loss at the joint interfaces (Fig. 6). The bond failures at the beginning of cyclic load applications are captured from the strain gauge readings shown in Fig. 7. The strain reading on the top and bottom surface of the bar shows strain reading of the bar at the bar and concrete boundary. In this figure, it can be observed that the strain gauges placed close to the joint faces (that is, 600 and 900 mm [24 and 36 in.]) recorded a higher value. The strain value reading reduces as the position shifts farther away from the joint faces. Although the strain value reduces as the distance moves further from the joint interface, the measured strain

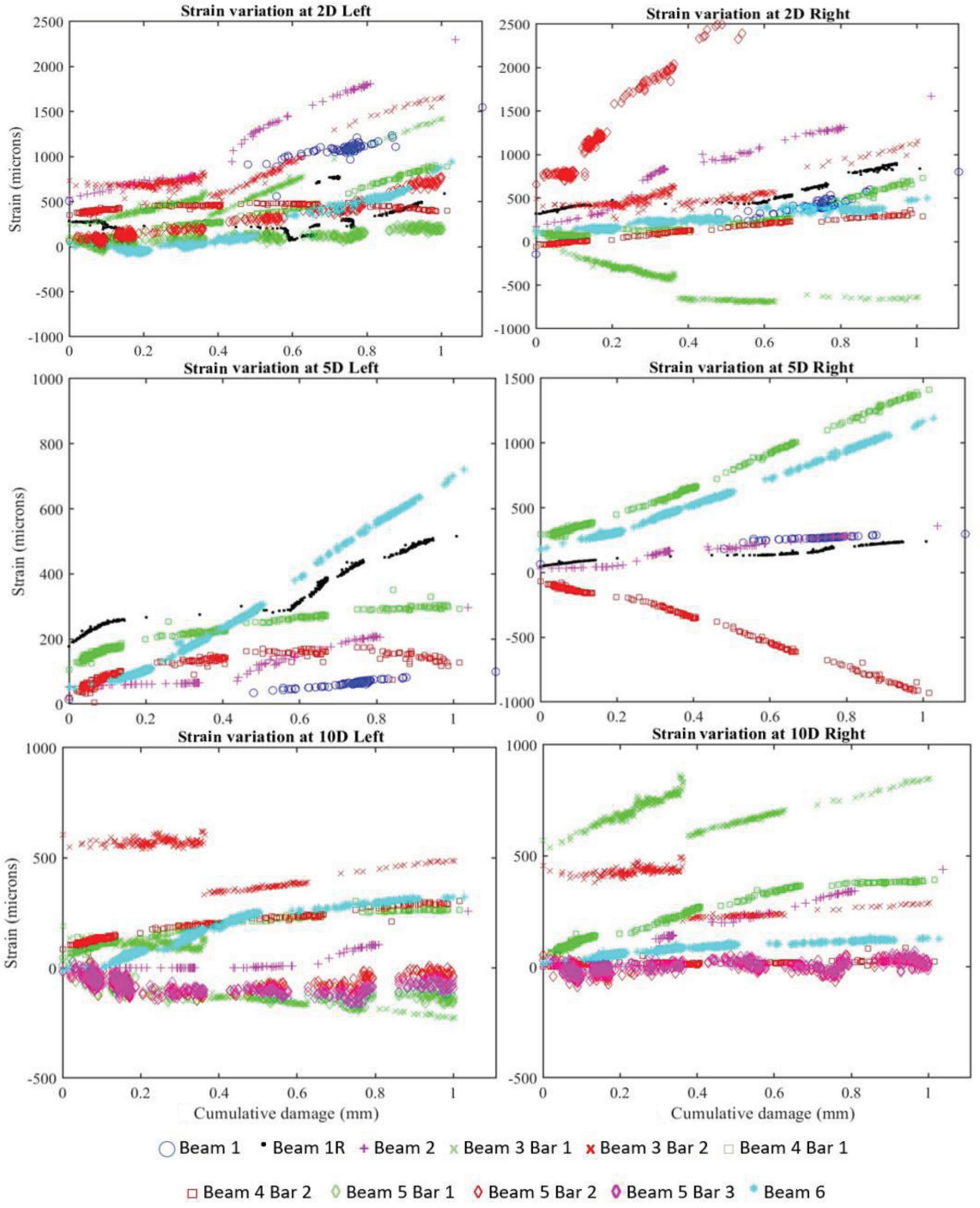

Fig. 7—Strain gauge readings of specimens at 1 mm (0.0394 in.) cumulative damage.

values on each location are incremental (Fig. 7). In addition, the strain values at the same location are different for the left and right units of the specimen. For specimens with more than one bar, the strain values at specific locations are not equal. This variation can be due to the internal stress distribution within the section and the redistribution of loads between the left and right units. In general, the strain readings of the specimens both at 2*D*, 5*D*, and 10*D* demonstrate that the sections undergo bond deterioration propagating from the joint face (Fig. 7). Bond degradation was recorded in investigations by Moradi et al.[7] and Maekawa and Qureshi[3] where the bond deterioration zone is the resulted because of the curvature formation under combined axial and shear loading conditions. Even though no direct axial load is applied to the specimens, similar behavior is observed in the set of experiments conducted.

Figure 8 illustrates the cycle endurance of each specimen under varying applied load levels. The applied load is normalized by its dowel capacity and considering that the load is distributed to both left and right units, the capacities computed in Table 2 are doubled. A comparative analysis is conducted with the control unit (Beam 1) to examine the influence of load level, bar size, confinement conditions, cross section size and compressive strength on the interfacial properties of joints during both the initiation and propagation stage. As explained earlier, the initiation stage is attributed to

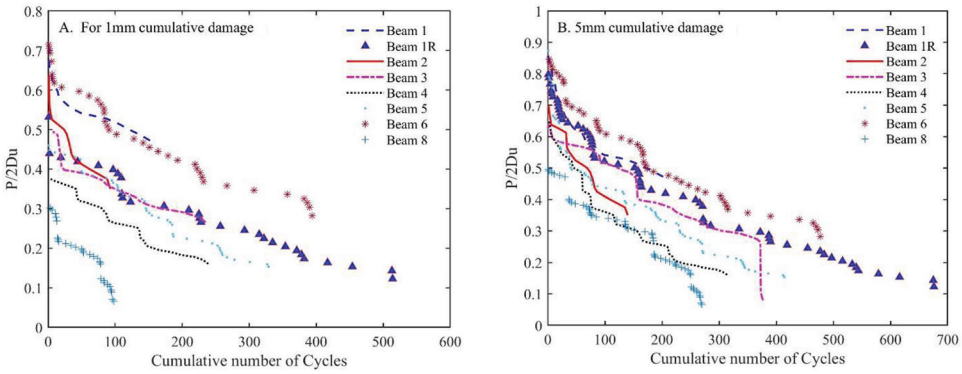

Fig. 8—Number of cycles specimens withstand for 1 and 5 mm (0.0394 and 0.1979 in.) cumulative damage, respectively; normalized load with critical dowel capacity.

the bond deterioration stage. The impact of load levels can be examined through the analysis of Beams 1 and 1R. Beam 1 experiences higher load amplitude during initial cycles, whereas Beam 1R is subjected to lower load amplification at the early stage of the cycle. As depicted in Fig. 8, in both the initiation and propagation stages, applying higher amplitude loading has demonstrated a reduction in fatigue life, while lower amplitude has exhibited an extension of fatigue life. The influence of bar types can be evaluated through the examination of Beams 1 and 2. Figure 8 distinctly illustrates that deformed bars (bar lugs) exhibit enhanced fatigue performance when compared to plain bars. The assessment of bar size is conducted through the study of Beam 3, revealing that adopting a smaller bar size leads to an early bond deterioration stage (Fig. 8(a)). Conversely, employing smaller bar sizes results in a higher fatigue life during the propagation stage (Fig. 8(b)). The issue of confinement can be addressed by looking into Beams 5 and 6. In the initiation stage, passive confinement (Beam 6) increases the fatigue life whereas active confinement has not so much improved the fatigue life. In the propagation stage, both confinement cases improve the fatigue life. Additionally, the effects of cross section increase and higher compressive strength are addressed using Beams 4 and 8 respectively. The size effect (Beam 4) has shown to shorten the fatigue life at both stages. Similarly, the mortar specimen (higher compressive strength) negatively impacts the fatigue life.

In Fig. 8, the slope of each specimen (except Beam 8) exhibits similar characteristics and hence poses similar fatigue rates. Upon scrutinizing the fatigue rate, a discernible trend in the slope of the graph is observed, excluding Beams 2 and 8, during the initiation stage. In the propagation stage, it can be generally fitted onto a similar slope, with the exception of Beam 2. Consequently, despite the variability in amplitude loading, a similarity in the sections is obtained based on fatigue resistance. The significant drop in fatigue rate for Beam 8 is attributed to coarse aggregate distribution in the mixture.[8]

Curvature formation

The examination of bond effects on curvature formation involves the careful selection of specimens—namely Beams 1, 2, and 7—as integral components of the investigation process. The selection of these three beams is intended to illustrate the influence of varying bond conditions on the degradation of concrete sections. Beam 7 is built to have a no-bond zone; this is done by covering the bar with rubber. In addition, the bar is on elastic subgrade due to the presence of layered rubber underneath the bar. Beam 7 is subjected to monotonic loading up to failure. The specimen showed a splitting crack at the top and bottom face; in addition, a significant slip of the end of the bar is also observed[9] (Fig. 6). The impact of such bond loss on the curvature formation can be understood from Fig. 9. Herein, the curvature value at 2*D* from the joint face is computed for Beams 1, 2, and 7. These values are compared with the theoretical curvature according to beam theory. The curvature of the section shown in Fig. 9 is computed when the section is loaded with half of its dowel capacity. In the case of Beam 7, the critical dowel capacity of Beam 1 can be considered. The effect of bond loss is shown to increase the curvature value. Beam 7 exhibits a higher curvature value, followed by Beam 2, where plain bars are used. Beam 1 has a lower curvature as compared to Beams 7 and 2. The formation of curvature plays an important role in the propagation stage. After the bond deterioration stage the crack propagation stage rampantly progresses through the section when plain bars are used. This crack propagation is attributed to the localized kinking (bending) of the bars (Fig. 6).

SUMMARY AND CONCLUSIONS

Experimental investigations of the joint interface under different conditions of confinement and bar arrangement are carried out. The cyclic load *P* applied to the center unit causes bond deterioration. This bond deterioration causes concrete deterioration in the specimens before any of the specimens reach the dowel capacity. Hence, joints are the crucial area that significantly reduces expected performance structures. The performance of joints depends on the confinement of the longitudinal bar. The provision of stirrups retards the formation of splitting cracks and lengthen the fatigue life. The following concluding remarks are made.

1. The cyclic shear force applied to the joints causes bond deterioration causing premature concrete deterioration.

2. When subjected to loads less than the dowel capacity, incremental plasticity due to concrete damage is observed in the jointed specimens.

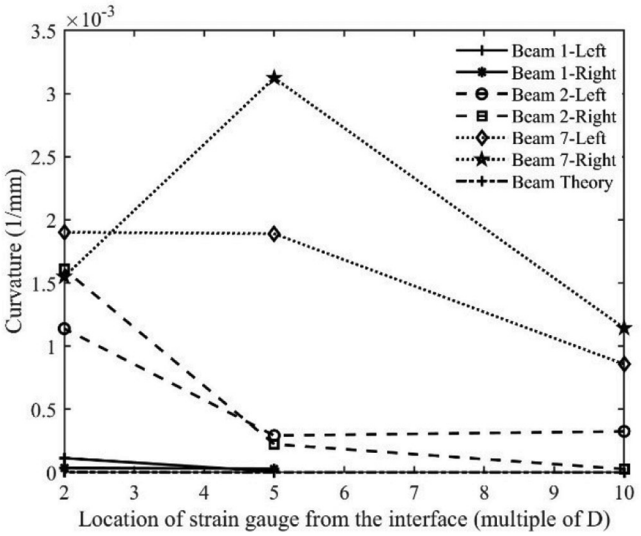

Fig. 9—Curvature distribution for different bond conditions.

3. The type of joint concrete deterioration depends on the confinement type, bar size, and load level.

4. For the unconfined sections, cracking occurs at the joint interface both below and above the bars, resulting in splitting cracks on the top and bottom surfaces of the specimens.

5. Confined sections exhibit concrete deterioration near the joint interface.

6. The curvature of the bar near the joint interface depends on the bond condition of the joint and the type of bar.

7. In this investigation, incremental deformation within the section identifies that a beam on an elastic foundation may not function for modeling dowel action under cyclic conditions.

AUTHOR BIOS

ACI member **Edom A. Zewdie** *is a PhD Candidate at Yokohama National University, Yokohama, Japan. She received her BSc and MSc in civil engineering from Addis Ababa University, Addis Ababa, Ethiopia, in 2013 and 2015, respectively. Her research interests include working on the shear-transfer mechanism due to dowel bars, focusing on the failure mechanism arising from bond degradation.*

Chikako Fujiyama *is a Professor at Yokohama National University. She received her BSc from Kyoto University, Kyoto, Japan, and MSc and PhD in civil engineering from The University of Tokyo, Tokyo, Japan. Her research interests include the mechanics of steel-concrete composite structures under cyclic loads and material development of geopolymer concrete.*

ACI member **Koichi Maekawa** *is an Emeritus Professor at The University of Tokyo and a Visiting Professor at Yokohama National University. He received his BSc, MSc, and PhD in civil engineering from The University of Tokyo. His research interests include multi-scale modeling of reinforced concrete structures both in mechanical and durability aspects.*

ACKNOWLEDGMENTS

The first author is grateful to the Monbukakusho (Ministry of Education, Culture, Sports, Science and Technology of the Japanese Government) for sponsoring postgraduate studies.

NOTATION

A_s	=	area of reinforcement bar
D	=	reinforcement bar diameter
D_u	=	critical dowel capacity
D_{ud}	=	design dowel capacity
f_{ck}	=	characteristics compressive strength
f_{yk}	=	characteristic *s* yield strength
N'	=	axial load or confining pressure
S	=	bar pullout displacement
V	=	shear force
δ	=	vertical deflection or shear displacement
δ_b	=	bar deflection
Φ	=	curvature of reinforcement bar
Φ_{max}	=	maximum curvature of reinforcement bar
τ_c	=	shear stress of concrete
τ_s	=	shear stress of reinforcement bar
σ_c	=	compressive stress developed on crack
σ_s	=	normal stress at reinforcement bar
$\overline{\omega}$	=	mean crack opening
ω_s	=	surface crack opening

REFERENCES

1. Randl, N., "Design Recommendations for Interface Shear Transfer in *fib* Model Code 2010," *Structural Concrete*, V. 14, No. 3, 2013, pp. 230-241. doi: 10.1002/suco.201300003

2. Maekawa, K.; Okamura, H.; and Pimanmas, A., *Non-Linear Mechanics of Reinforced Concrete*, CRC Press, London, UK, 2003, pp. 385-431.

3. Maekawa, K., and Qureshi, J., "Computational Model of Reinforcing Bar Embedded in Concrete Under Combined Axial Pullout and Transverse Displacement," *Doboku Gakkai Rombunshuu*, V. 31, No. 538, 1996, pp. 227-239. doi: 10.2208/jscej.1996.538_227

4. Vintzēleou, E. N., and Tassios, T. P., "Mathematical Models for Dowel Action Under Monotonic and Cyclic Conditions," *Magazine of Concrete Research*, V. 38, No. 134, 1986, pp. 13-22. doi: 10.1680/macr.1986.38.134.13

5. Timoshenko, S., *Strength of Materials, Part II: Advanced Theory and Problems*, third edition, D. Van Nostrans Company, Inc., 1956, 563 pp.

6. Vintzeleou, N., and Tassios, T. P., "Behavior of Dowels under Cyclic Deformations," *ACI Structural Journal*, V. 84, No. 1, Jan.-Feb. 1987, pp. 18-30.

7. Moradi, A. R.; Soltani, M.; and Tasnimi, A. A., "A Simplified Constitutive Model for Dowel Action Across RC Cracks," *Journal of Advanced Concrete Technology*, V. 10, No. 8, 2012, pp. 264-277. doi: 10.3151/jact.10.264

8. Zewdie, E.; Fujiyama, C.; and Maekawa, K., "Performance of Precast Concrete Joints in Cyclic Shear By Using Prepacked Concrete," *Journal of Japan Concrete Institute*, V. 45, 2023.

9. Zewdie, E., and Maekawa, K., "Failure and Limit States of Precast Concrete Joints Under Low Cycle Shear," *Proceedings of the 14th* fib *International PhD Symposium in Civil Engineering*, Rome, Italy, 2022, pp. 81-88